Spatial migration of earthquakes within seismic clusters in Southern California: Evidence for fluid diffusion

X. Chen,[1] P. M. Shearer,[1] and R. E. Abercrombie[2]

Received 25 October 2011; revised 30 January 2012; accepted 10 February 2012; published 3 April 2012.

[1] Seismicity within many earthquake swarms is observed to migrate slowly with time, which may reflect event triggering due to slow fault slip or fluid flow. We search for this behavior in Southern California by applying a weighted least squares method to quantify event migration within 69 previously observed seismicity bursts. We obtain best-fitting migration directions and velocities, and compute a statistical migration significance s_m for each burst using a bootstrap resampling method. We define 37 bursts with $s_m \geq 0.8$ as the migration group, and 32 bursts with $s_m < 0.8$ as the non-migration group. To explore differences between the two groups, for each burst we compute effective stress drop ($\Delta\sigma_{quasi}$, the ratio between total moment and radius), the skew of the moment release time series (μ), the timing of the largest event ($t_{\max}$), and the distance separation between the first half and second half of the sequence (d_s). As expected, the migration group features larger d_s and lower $\Delta\sigma_{quasi}$, consistent with higher migration significance. It also features lower μ and higher $t_{\max}$, similar to observations from swarms in the Salton Trough, while the non-migration group is more similar to main shock-aftershock sequences. To explore possible fluid involvement, we model the migration behavior with the fluid diffusion equation, and identify 18 bursts with diffusion coefficients ranging from 0.01 to 0.8 m^2/s, with the majority below 0.16 m^2/s. The obtained diffusion coefficients and migration behavior are similar to the Reservoir-induced seismicity beneath the Açu reservoir in Brazil. The majority of normal faulting events are associated with these 18 bursts, while the non-migration group has the most reverse faulting events, indicating a possible link between sequence type and focal mechanism.

Citation: Chen, X., P. M. Shearer, and R. E. Abercrombie (2012), Spatial migration of earthquakes within seismic clusters in Southern California: Evidence for fluid diffusion, *J. Geophys. Res.*, *117*, B04301, doi:10.1029/2011JB008973.

1. Introduction

[2] Earthquakes are observed to strongly cluster in time and space. Two major sources for earthquake clustering are main shock-aftershock sequences and swarms. Aftershock sequences are triggered directly or indirectly by a large earthquake near the beginning of the sequence, while earthquake swarms do not have obvious main shocks, and are thought to be mainly triggered by an underlying physical processes, such as fluid flow or aseismic slip. Fluid involvement is commonly observed for volcanic swarms, for which the spatial-temporal evolution of seismicity and earthquake source properties (focal mechanism, spectral characteristics, etc.) are consistent with magma movement [e.g., *Hough et al.*, 2000; *Hayashi and Morita*, 2003; *Yukutake et al.*, 2011]. Fluids are also common drivers for non-volcanic swarms within geothermal regions or induced by impoundment of reservoirs [e.g., *Kato et al.*, 2010; *El Hariri et al.*, 2010; *Daniel et al.*, 2011]. The occurrence of induced seismic swarms during injection experiments is a strong indicator of fluid triggering, e.g., at the Coso geothermal field [*Julian et al.*, 2010]. Aseismic slip as a driving force has been observed for a swarm within the Salton Trough [e.g., *Lohman and McGuire*, 2007]. Most earthquake swarms exhibit spatial migration of a seismicity front [e.g., *Roland and McGuire*, 2009; *Chen and Shearer*, 2011], and this migration behavior can help to distinguish between different triggering mechanisms. The fluid-involved swarms can be modeled as a diffusion process, with diffusivity ranging from 0.02 to about 10 m^2/s [e.g., *do Nascimento et al.*, 2005; *Shapiro et al.*, 2005; *Parotidis et al.*, 2005; *Talwani et al.*, 2007].

[3] *Vidale and Shearer* [2006] (VS2006) investigated 71 seismic bursts across Southern California based on a waveform-relocated catalog. They classified the bursts into 'swarm-like', 'aftershock-like' and 'mixed' categories according to the timing of the largest event in each sequence. They argued that the strong spatial expansion of 'swarm-like' bursts can be explained by fluid diffusion processes, but that the steady rate of seismicity during many swarms

[1]Scripps Institution of Oceanography, University of California, San Diego, La Jolla, California, USA.
[2]Department of Earth Sciences, Boston University, Boston, Massachusetts, USA.

0148-0227/12/2011JB008973

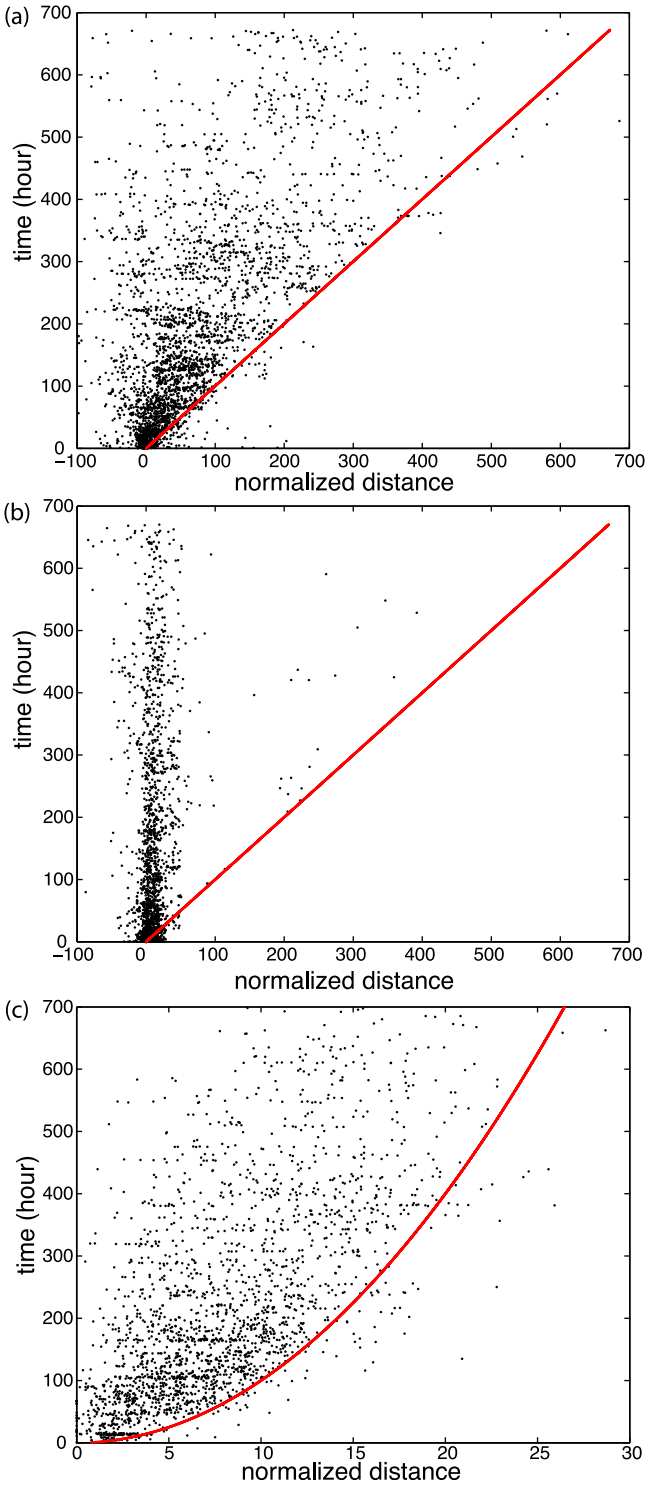

Figure 1. (a) Stacked time versus normalized distance migration behavior for 37 bursts with migration significance ≥0.8. (b) Stacked normalized migration behavior for 32 bursts with migration significance <0.8. (c) Stacked normalized diffusion migration curve for 18 bursts. Red lines in Figures 1a and 1b represent normalized distance following $d = t - t_0$, red line in Figure 1c represents normalized distance following $d = \sqrt{t - t_0}$.

was more consistent with aseismic slip episodes. *Chen and Shearer* [2011] (CS2011) developed a weighted least squares method to model the migration of seismicity onsets, and used the best-fitting migration velocities and directions to distinguish between swarms driven by fluid flow and aseismic slip. Pore fluid diffusion is typically at velocities on the order of m/day, generally much slower than aseismic slip-driven migration, which is usually at km/hour [*Roland and McGuire*, 2009]. In this study, we take advantage of the LSH catalog [*Lin et al.*, 2007] which features high resolution within similar event clusters, to update the locations of the 71 bursts identified in VS2006, and apply the migration analysis procedure from CS2011 to these bursts. The waveform-relocated catalog for the reservoir-induced seismicity (RIS) beneath the Açu reservoir in Brazil (henceforth referred to as the Brazil swarm), previously analyzed in detail [*do Nascimento et al.*, 2004, 2005; *El Hariri et al.*, 2010], is also included in our analysis for comparison. Our results help clarify the differences among earthquake bursts and their origins, and provide evidence for fluid migration as the driving force behind many swarms in southern California.

2. Migration Behavior

[4] With updated locations, 2 out of the 71 original bursts have too few events to properly analyze (fewer than 10 events). For the remaining 69 bursts, we apply the weighted least squares method to model the linear migration of seismicity onset times (i.e., the lower edge of the upper-triangle function in time versus distance plots of seismicity), to compute the best-fitting migration directions and velocities, following the equation $t = t_0 + \vec{n}\cdot(\vec{X} - \vec{X_0})/v$, where $\vec{n}$ is the migration direction, v is migration velocity, t_0 is the timing of the first event, and $\vec{X}_0$ is the location of the first event. The estimated velocities generally appear slower than swarms within the Salton Trough (henceforth referred to as SS-swarms) (CS2011), and are mostly below 0.01 km/hour. We then apply a statistical resampling method to obtain a statistical significance (s_m) for the migration behavior of each burst. This method works by randomly 'scrambling' the occurrence time of each event in the sequence, and then applying the least squares method to find the minimum misfit for each resampled data set. This procedure is repeated 100 times for each burst, and s_m is defined as the percentage of higher misfits from the resampled data set compared with the original data set. The computed s_m values range from 0.5 to 1.0 for all bursts, with generally higher values for the 18 'swarm-like' bursts in VS2006 and lower values for the 'aftershock-like' bursts. We separate the 69 bursts into two groups based on s_m, in which 37 bursts (including 14 'swarm-like' bursts) with $s_m \geq 0.8$ are defined as the migration group, and 32 bursts (including 12 'aftershock-like' bursts) with $s_m < 0.8$ are defined as the non-migration group. For each burst, we compute the normalized distance using $d_n = \vec{n}\cdot(\vec{X} - \vec{X_0})/v$ with the best-fitting migration direction ($\vec{n}$) and velocity (v). To illustrate differences in the migration behavior among each group, we combine (stack) data from all bursts within the same group, and plot normalized distance versus time for each event. Shown by Figure 1a, the seismicity onset of the migration group aligns well with the best-fitting straight line, while the seismicity of the non-

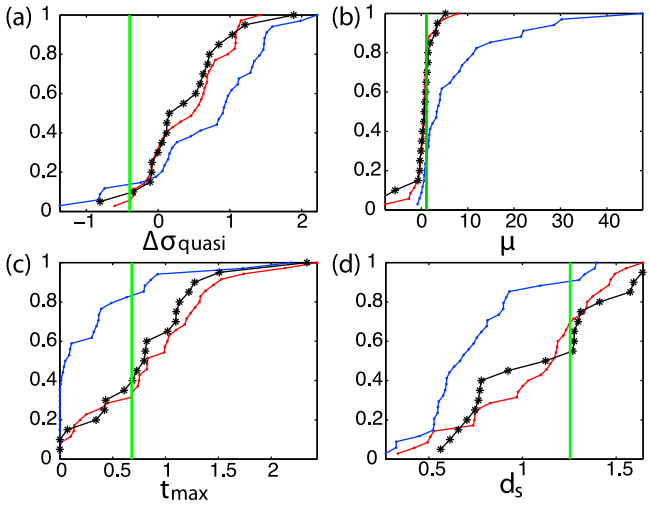

Figure 2. Cumulative distribution functions (CDFs) for different burst categories, as a function of (a) effective stress drop (log scale), (b) skew of seismic moment release, (c) time delay of the largest event normalized by the mean time delay, and (d)the normalized distance separation between the first and second half of the burst. Results for swarms in the Salton Trough from *Chen and Shearer* [2011] are shown in black, bursts from *Vidale and Shearer* [2006] with $s_m \geq 0.8$ are shown in red, bursts with $s_m < 0.8$ are shown in blue, results for the Brazil swarm are shown in green.

migration group (Figure 1b) centers within a narrow region regardless of time. The uncertainty of migration directions within the migration group is estimated to be 15° with respect to the median value from the resampling method.

3. Statistical Characteristics

[5] The overlap with the categories in VS2006 indicates the migration group is similar to swarms, while the non-migration group is similar to main shock-aftershock sequences. To explore differences between the two groups, we compute a set of parameters for each of the bursts, and identify differences among the statistical distributions within each group. Similar to the SS-swarms, we compute the parameter $t_{\max}$, which is the time delay of the largest event normalized by the mean time delay within the burst. We also compute the skew of the seismic moment release μ, calculated from the third moment and standard deviation of the seismic moment time history (details in CS2011). μ is generally lower for swarms, and higher for aftershock sequences [*Roland and McGuire*, 2009]. In addition to these two parameters associated with the event magnitude, we compute two other parameters to quantify the spatial distribution of the bursts. Parameter $\Delta\sigma_{quasi} = \frac{7\sum_1^n M_0^i}{16r^3}$ (r is the mean radius of the burst) quantifies the total moment release relative to the area of the burst. *Roland and McGuire* [2009] showed that swarms on transform faults generally have lower $\Delta\sigma_{quasi}$ and lower μ compared with main shock-aftershock sequences. Another parameter, d_s, measures the distance separation between the centers of the first half and second half of each burst, normalized by the mean radius of the burst, which provides an alternate measurement of the spatial migration.

[6] We compute the parameters $t_{\max}$, μ, $\Delta\sigma_{quasi}$ and d_s for the 69 bursts, and compare the CDF (cumulative density function) of the distribution for each parameter. For comparison, we also compute the same parameter set for the SS-swarms and the Brazil swarm. The Brazil swarm features μ of 1.1, $t_{\max}$ of 0.7, d_s of 0.5, and $\Delta\sigma_{quasi}$ of 0.4, close to the median values for the migration group and SS-swarms, with a slight lower $\Delta\sigma_{quasi}$. Shown in Figure 2, the migration group has similar parameter distributions to the SS-swarms. For μ (Figure 2b), we find that the SS-swarms and the migration group have very similar distributions, which are limited to a range between −3 and 5, while the non-migration group extends from 0 to about 45. Higher μ values indicate the energy release is concentrated at the beginning of the sequence, consistent with lower $t_{\max}$ for the non-migration group (see Figure 2c). Figure 2d shows the distance separation between the first and second halves for the SS-swarms. As expected, this separation is much greater for the migration group than the non-migration group.

[7] For the $\Delta\sigma_{quasi}$ parameter (Figure 2a), the SS-swarms and the migration group have median values around 3 MPa, while the non-migration group has median values around 8 MPa, higher than the other two groups, which indicates the total moment release is centered in a relatively small region. To investigate whether the $\Delta\sigma_{quasi}$ values have any relationship to stress drops for individual earthquakes, we compare the values with stress drop estimates ($\Delta\sigma$), available for some of the events from *Shearer et al.* [2006]. We find 39 bursts have at least 10 events with stress drop estimates, of which 21 bursts fall within the migration group and 18 within the non-migration group. We compute the correlation coefficient and significance of correlation between $\Delta\sigma_{quasi}$ and median $\Delta\sigma$ based on a t-test. We apply a bootstrap method to obtain the distribution of correlation coefficients and the significance based on 1000 resampled data sets. Including all bursts, the correlation coefficient between $\Delta\sigma_{quasi}$ and median $\Delta\sigma$ is 0.1, and is only significant at the 50% confidence level. For the migration group, the correlation is around 0.4, and is significant at over 90% confidence; however, the non-migration group has a slightly negative correlation of −0.15 at a confidence level of 50%. For comparison, the SS-swarm has a coefficient of 0.4 at a confidence level of 90%, similar to the migration group. The correlation results show that the 'swarm-like' migration group is more correlated to the average single event stress drop estimates, although not very strongly, while the 'aftershock-like' non-migration group is barely correlated at all. The rupture area and the total moment for a main shock-aftershock sequence is mostly dominated by the main shock, so $\Delta\sigma_{quasi}$ should approximate the main shock stress drop, and not necessarily correlate to individual aftershock stress drops. Unfortunately, due to waveform clipping problems, the *Shearer et al.* [2006] study does not include stress drop estimates for events larger than about M 3.5, so we cannot compare our results directly to main shock stress drops.

[8] Another important feature is the deviation of the temporal event distribution from Omori's power law decay curve. Individual bursts exhibit variations in their temporal distributions, so to examine the general features of the two groups, we stack the delay times in each burst relative to the

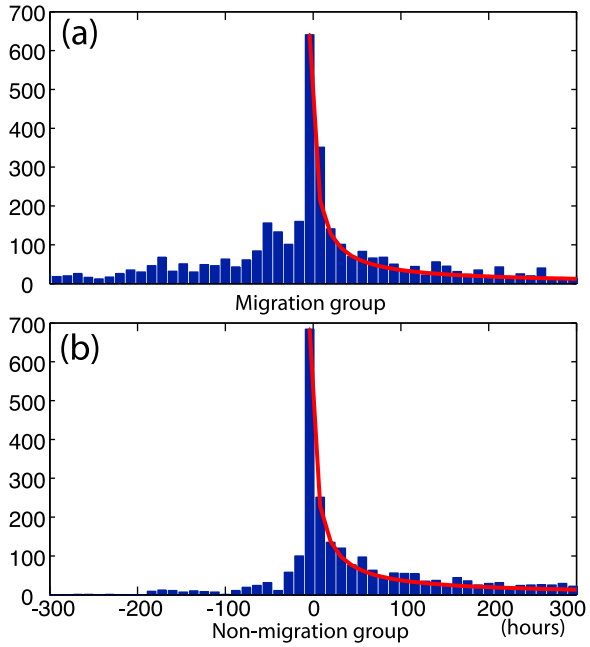

Figure 3. (a) Temporal distribution for events within bursts with high migration significance ($s_m \geq 0.8$). (b) Temporal distribution for bursts with low migration significance ($s_m < 0.8$). Red lines are the predicted t^{-1} decay curves.

largest event within each group. Figure 3 shows that the migration group has about 50% of its seismicity before the largest event, while the non-migration group is more similar to typical main shock-aftershock sequences with very few events prior to the largest event. Despite the differences in the 'foreshocks' before the largest event, both groups exhibit power law decay after the largest event in each sequence. The temporal distributions of SS-swarms and the Brazil swarm are similar to the migration group with an excess of seismicity before the largest event and Omori-like decay afterward. Such Omori-like decay indicates that some earthquake-to-earthquake triggering is likely significant even for the migration group [*Hainzl and Ogata*, 2005]; however, it should be noted that individual bursts do not usually follow Omori-like decay as closely as the stacked result.

4. Fluid Diffusion

[9] In CS2011, the possibility of fluid movement as a driving force is analyzed for some swarms within the Salton Sea geothermal field, where continuous injection and production are conducted. To investigate possible fluid involvement for the 69 bursts, we apply the same fluid diffusion modeling procedure used in CS2011. We use a similar weighted least squares method to find the best-fitting diffusion coefficient based on the migration of seismicity onset, following the equation $|\vec{X}-\vec{X_0}| = \sqrt{4\pi D(t-t_0)}$, where D is the diffusion coefficient. To apply the least squares method, we modify the equation to $t = t_0 + |\vec{X}-\vec{X_0}|^2/(4\pi D)$, and solve for D. A similar resampling method is used to find the statistical significance s_m. For each burst, we apply a bootstrap method to compare the misfit from the two models. The least squares procedures are applied to 100 resampled data sets, and the misfits from the two models are compared for each data set. We find 18 bursts have overall lower misfits with the diffusion model, which are all within the previously defined migration group of 37 bursts. We consider these 18 bursts as likely driven by fluid diffusion, of which 15 bursts have diffusion coefficients ranging from 0.01 to 0.16 m^2/s and 3 bursts have higher coefficients from 0.4 to 0.8 m^2/s. The uncertainty of the coefficients is estimated to be about 10% from the bootstrap test. Of the 6 bursts within the Coso geothermal field, 4 are better fit with the fluid diffusion curve, similar to previous observations in the Salton Sea geothermal field, which indicated a high fraction of swarms that are fit with the diffusion curve (CS2011). To illustrate the diffusive migration behavior, we normalize distance using $d_n = |\vec{X}-\vec{X_0}|/\sqrt{4\pi D}$, and combine (stack) the 18 bursts to produce a distance versus time plot, shown in Figure 1c.

[10] We also compare these results with the Brazil swarm, which was triggered by increased water level in the Açu Reservoir [*El Hariri et al.*, 2010]. We apply both the linear migration model and diffusion migration model to the waveform relocated catalog and compare the misfit from the two models. The migration significance is over 95% for both models, and the misfit from diffusion modeling is much lower than the linear migration model, consistent with a fluid triggering mechanism. We obtain a linear migration velocity of 38.4 m/d during peak seismicity, consistent with the velocity of 32–52.5 m/d obtained by *El Hariri et al.* [2010], and a diffusion coefficient of about 0.02 m^2/s, somewhat lower than the hydraulic diffusivity of 0.06 m^2/s obtained by *do Nascimento et al.* [2005], but within the same

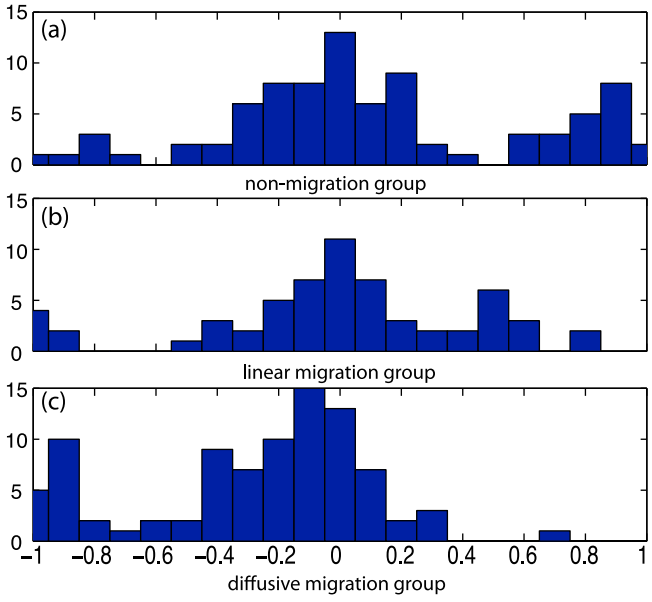

Figure 4. Focal mechanism distribution for events within (a) the non-migration group, (b) the linear migration group, and (c) the fluid diffusion group. Here −1 corresponds to normal faulting, 0 corresponds to strike-slip faulting, and 1 corresponds to reverse faulting.

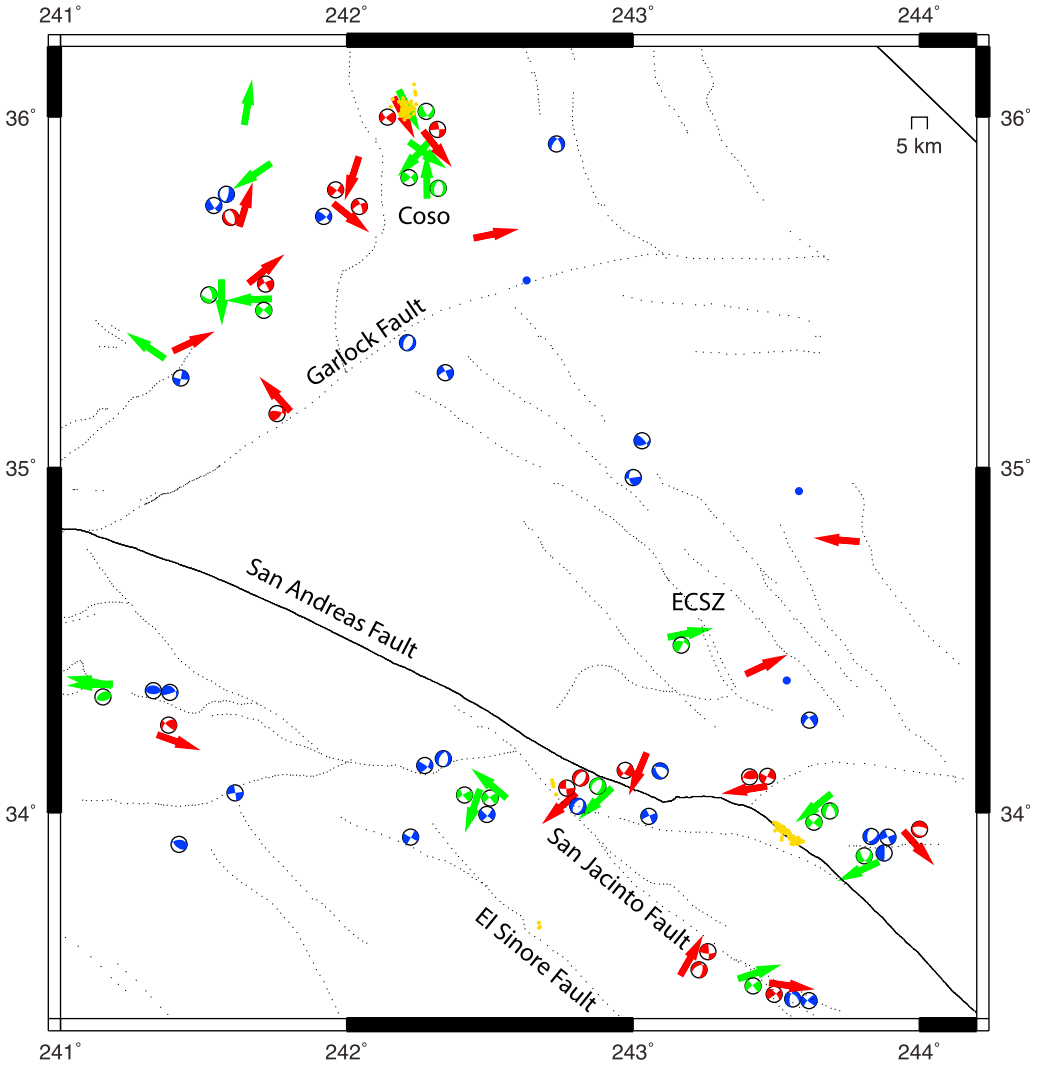

Figure 5. Map view of burst locations, major focal mechanisms and migration directions. Yellow dots are the geothermal well locations (data from California Conservation Department website). Arrows are the best-fitting directions for bursts within the migration group. Green color indicates bursts best fit with diffusion curves. Red color indicates bursts with $s_m \geq 0.8$. Blue color indicates bursts with $s_m < 0.8$ and no clear migration directions. Focal mechanisms are from *Hardebeck and Shearer* [2003], the focal type of the largest available earthquake and second largest available earthquake with a different focal type are plotted for each burst. If no focal mechanism or migration is available for a burst, a dot of corresponding color is plotted.

order, considering the wide range of diffusivities that have been reported [e.g., *Talwani et al.*, 2007].

5. Focal Mechanisms

[11] So far, we have identified three types of bursts, the non-migration 'aftershock-like' bursts, linear migrating bursts, and bursts with apparent fluid involvement. VS2006 found that normal faulting mechanisms are usually associated with 'swarm-like' bursts, while 'aftershock-like' bursts are mainly associated with strike-slip and thrust faulting mechanisms. Here, we associate events from each burst with focal mechanism solutions from the HASH catalog [*Hardebeck and Shearer*, 2003], and then compute the focal mechanism type using the same method as VS2006, where −1 is normal faulting, 0 is strike-slip faulting and 1 is reverse faulting. We use focal mechanism solutions with quality A and B, and find 46 out of 69 bursts have at least one focal mechanism. We then separate the events into the three groups based on the burst type. As shown in Figure 4, the non-migration group has the most reverse faulting mechanisms, the linear migration group is dominated by strike-slip faulting mechanisms, while the fluid-driven bursts have an excess of normal faulting mechanisms. Roughly speaking, about 70% of the reverse faulting events belong to the non-migration group and about 60% of the normal faulting events belong to the diffusive group. Strike-slip faulting is the dominant mechanism among all

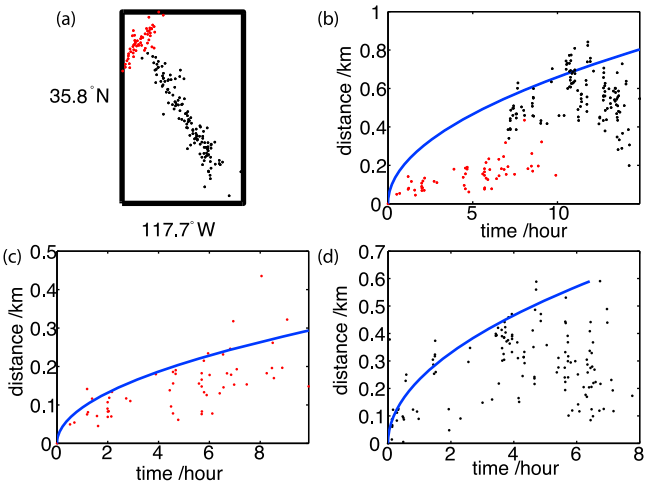

Figure 6. (a) Map view of events within a swarm starting on 08/01/1992 in Coso geothermal field. (b) Best-fitting diffusive migration curve for all events with D = 0.04 m^2/s. (c) Best-fitting diffusive curve for the NE-SW striking events at the early stage of the swarm with D = 0.008 m^2/s. (d) Best-fitting diffusive curve for the SE-NW striking events at the later part of the swarm with D = 0.05 m^2/s. Red dots correspond to events in Figure 6c, black dots corresponds to events in Figure 6d. Blue lines in Figures 6b–6d are the predicted migration curve with corresponding diffusion coefficients in each figure. Distance in Figures 6b–6d is relative to the first event in each figure.

events, events of this type are evenly distributed among the three groups, and it is also the dominant focal mechanism among events in the SS-swarms and the Brazil swarm. Because these results could be dominated by a few large bursts, we also find the most common focal type and the focal type of the largest event with a focal mechanism solution for each burst. The results consistently show that the fluid-involved swarms have a higher fraction of normal-faulting mechanisms. As shown in Figure 5, south of the Garlock Fault, the fluid associated bursts are mostly distributed within the San Jacinto Fault Zone, the San Andreas Fault-Coachella zone, and the Eastern California Shear Zone, where high focal mechanism heterogeneity and substantial normal faulting are found [*Bailey et al.*, 2010]. However, the higher fraction of reverse faulting seen within the non-migration group is not obvious, as both the linear migrating swarms and the non-migration group are dominated by strike-slip faulting mechanisms.

[12] We also compare the migration directions with focal mechanism orientations of the largest event in each burst. The migration directions are mostly at about 5° to 30° to one of the best-fitting focal planes, and are mostly within 30° of the seismicity strike direction. Considering the uncertainty of 15° for the migration direction estimates, this result indicates rough agreement between the focal mechanism orientations and migration directions. However, the directions usually do not follow surface fault traces, especially for the fluid associated bursts (see Figure 5), which include most normal faulting components. As noted by *Bailey et al.* [2010], for non strike-slip faulting types, the dominant focal mechanism orientations usually do not agree with surface traces, and may sample secondary fault structures.

6. Discussion

[13] There have been many studies on fluid diffusivity using migration of microseismicity within geothermal areas, gas field, rift, volcanic regions, etc. *Talwani et al.* [2007] analyzed over 90 cases of induced seismicity from reservoir and geothermal injection experiments, and found the hydraulic diffusivities lie between 0.1 and 10 m^2/s. *Shapiro et al.* [2005] obtained a diffusivity of 0.023 m^2/s by fitting seismicity fronts triggered during a hydraulic fracturing test in Soultz (France), which is consistent with the diffusivity obtained based from a borehole injection/flow test. The diffusivities for Southern California are mostly between 0.01 and 0.16 m^2/s, consistent with values for other geothermal regions (obtained from hydraulic fracturing tests), water reservoirs and rift-related swarms, which range between 0.02 to 0.25 m^2/s [*Audigane et al.*, 2002; *Shapiro et al.*, 2005; *do Nascimento et al.*, 2005; *Pacchiani and Lyon-Caen*, 2010]. The values are slightly lower than diffusivities obtained for volcanic regions, which are generally between 0.2 to 0.7 m^2/s [*Shapiro et al.*, 2005; *Parotidis et al.*, 2005; *Yukutake et al.*, 2011]. The diffusive bursts are mostly distributed between 0 and 15 km depth. There is a hint of decreasing diffusivity with depth between 2 and 6 km, but this trend is less clear for deeper bursts.

[14] Some swarms feature episodes with different diffusivities. *Parotidis et al.* [2005] obtained diffusivities ranging from 0.3 to 10 m^2/s for different episodes of seismicity during the 2000 Vogtland swarm, and suggested hydraulic heterogeneities as a possible cause. We find two swarms within the Coso geothermal region are best explained with two different diffusion curves, both starting with lower diffusivity and continuing with higher diffusivity. The swarm starting on 08/12/1984 began with lower diffusivity at shallower depth, and continued to deeper depths with a higher diffusivity; the swarm starting on 08/01/1992 began with lower diffusivity at deeper depth along a NE-SW strike, and continued to shallower depth at SE-NW strike with higher diffusivity (see Figure 6). The different migration behaviors within the same swarm may arise from different diffusivity patches that account for hydraulic heterogeneities.

[15] The linear migration velocities for swarms within the linear migration group are mostly below 0.01 km/hour, about an order of magnitude lower than the average migration velocities for the SS-swarm (CS2011) and swarms along transform faults [*Roland and McGuire*, 2009]. The typical aseismic slip velocity is on the order of 0.1 km/hour to 1.0 km/hour [*Roland and McGuire*, 2009, and references therein]. Our low observed velocities for these swarms are more comparable to fluid-driven migrations [e.g., *Hainzl and Ogata*, 2005], but we nonetheless achieve better data fits with a constant linear velocity than with a diffusion curve. Thus, these swarms may have been triggered by slower or weaker aseismic slip than previous work has suggested is typical for slow-slip events. Future analysis with Epidemic Type Aftershock Sequence (ETAS) models and physical seismicity models

based on rate and state friction laws may help to reveal additional information [e.g., *Hainzl and Ogata* 2005; *Llenos and McGuire*, 2011].

7. Conclusions

[16] We examine 69 seismicity bursts across southern California to quantify the spatial migration of their events and to explore differences in their behavior as defined by parameters that describe the time history of moment release and stress drop estimates. Bursts that do not exhibit significant migration (with migration significance $s_m < 0.8$) have low $t_{\max}$, low d_s, high μ and high $\Delta\sigma_{quasi}$, and are mostly aftershock-like sequences, while bursts with high s_m feature high $t_{\max}$, high d_s, low μ and low $\Delta\sigma_{quasi}$, are more 'swarm-like'. Through diffusive migration behavior modeling, we find over half of the migration bursts are better-fitted to a diffusive curve with similar parameters to a well-recorded RIS sequence, indicating fluid involvement, and the diffusivities are consistent with previous studies for geothermal reservoirs. The focal mechanism solutions for the fluid-involved bursts show a high fraction of normal faulting mechanisms, consistent with the hypothesis of an extensional stress field for geothermal reservoirs. Further analysis with ETAS modeling and physical models may help to further explain this behavior.

[17] **Acknowledgments.** We thank one anonymous Associate Editor and two anonymous reviewers for their suggestions and comments. This research was supported by the Southern California Earthquake Center.

References

Audigane, P., J. Royer, and H. Kaieda (2002), Permeability characterization of the Soultz and Ogachi large-scale reservoir using induced microseismicity, *Geophysics*, *67*(1), 204–211.

Bailey, I. W., Y. Ben-Zion, T. W. Becker, and M. Holschneider (2010), Quantifying focal mechanism heterogeneity for fault zones in central and southern California, *Geophys. J. Int.*, *183*, 433–450, doi: 10.1111/j.1365-246X.2010.04745.x.

Chen, X., and P. M. Shearer (2011), Comprehensive analysis of earthquake source spectra and swarms in the Salton Trough, California, *J. Geophys. Res.*, *116*, B09309, doi:10.1029/2011JB008263.

Daniel, G., et al. (2011), Changes in effective stress during the 2003–2004 Ubaye seismic swarm, France, *J. Geophys. Res.*, *116*, B01309, doi:10.1029/2010JB007551.

do Nascimento, A. F., P. A. Cowie, R. J. Lunn, and R. G. Pearce (2004), Spatio-temporal evolution of induced seismicity at Açu reservoir, NE Brazil, *Geophys. J. Int.*, *158*, 1041–1052.

do Nascimento, A. F., R. J. Lunn, and P. A. Cowie (2005), Modeling the heterogeneous hydraulic properties of faults using constraints from reservoir-induced seismicity, *J. Geophys. Res.*, *110*, B09201, doi:10.1029/2004JB003398.

El Hariri, M., R. E. Abercrombie, C. A. Rowe, and A. F. do Nascimento (2010), The role of fluids in triggering earthquakes: Observations from reservoir induced seismicity in Brazil, *Geophys. J. Int.*, *181*, 1566–1574.

Hainzl, S., and Y. Ogata (2005), Detecting fluid signals in seismicity data through statistical earthquake modeling, *J. Geophys. Res.*, *110*, B05S07, doi:10.1029/2004JB003247.

Hardebeck, J. L., and P. M. Shearer (2003), Using S/P amplitude ratios to constrain the focal mechanisms of small earthquakes, *Bull. Seismol. Soc. Am.*, *90*(6), 2434–2444.

Hayashi, Y., and Y. Morita (2003), An image of a magma intrusion process inferred from precise hypocentral migrations of the earthquake swarm east of the Izu peninsula, *Geophys. J. Int.*, *153*(1), 159–174.

Hough, S. E., R. S. Dollar, and P. Johnson (2000), The 1998 earthquake sequence south of Long Valley Caldera, California: Hints of magmatic involvement, *Bull. Seismol. Soc. Am.*, *90*(3), 752–763.

Julian, B. R., G. R. Foulger, F. C. Monastero, and S. Bjornstad (2010), Imaging hydraulic fractures in a geothermal reservoir, *Geophys. Res. Lett.*, *37*, L07305, doi:10.1029/2009GL040933.

Kato, A., S. Sakai, T. Iidaka, T. Iwasaki, and N. Hirata (2010), Non-volcanic seismic swarms triggered by circulating fluids and pressure fluctuations above a solidified diorite intrusion, *Geophys. Res. Lett.*, *37*, L15302, doi:10.1029/2010GL043887.

Lin, G., P. M. Shearer, and E. Hauksson (2007), Applying a three-dimensional velocity model, waveform cross correlation, and cluster analysis to locate southern California seismicity from 1981 to 2005, *J. Geophys. Res.*, *112*, B12309, doi:10.1029/2007JB004986.

Llenos, A. L., and J. J. McGuire (2011), Detecting aseismic strain transients from seismicity data, *J. Geophys. Res.*, *116*, B06305, doi:10.1029/2010JB007537.

Lohman, R. B., and J. J. McGuire (2007), Earthquake swarms driven by aseismic creep in the Salton Trough, California, *J. Geophys. Res.*, *112*, B04405, 10.1029/2006JB004596.

Pacchiani, F., and H. Lyon-Caen (2010), Geometry and spatio-temporal evolution of the 2001 Agios Ioanis earthquake swarm (Corinth Rift, Greece), *Geophys. J. Int.*, *180*(1), 59–72.

Parotidis, M., S. A. Shapiro, and E. Rothert (2005), Evidence for triggering of the Vogtland swarms 2000 by pore pressure diffusion, *J. Geophys. Res.*, *110*, B05S10, doi:10.1029/2004JB003267.

Roland, E., and J. J. McGuire (2009), Earthquake swarms on transform faults, *Geophys. J. Int.*, *178*, 1677–1690.

Shapiro, S. A., R. Susanne, and E. Rothert (2005), Characterization of hydraulic properties of rocks using probability of fluid-induced micro-earthquakes, *Geophysics*, *70*(2), 27–33.

Shearer, P. M., G. A. Prieto, and E. Hauksson (2006), Comprehensive analysis of earthquake source spectra in southern California, *J. Geophys. Res.*, *111*, B06303, doi:10.1029/2005JB003979.

Talwani, P., L. Chen, and K. Gahalaut (2007), Seismogenic permeability, ks, *J. Geophys. Res.*, *112*, B07309, doi:10.1029/2006JB004665.

Vidale, J. E., and P. M. Shearer (2006), A survey of 71 earthquake bursts across southern California: Exploring the role of pore fluid pressure fluctuations and aseismic slip as drivers, *J. Geophys. Res.*, *111*, B05312, doi:10.1029/2005JB004034.

Yukutake, Y., H. Ito, R. Honda, M. Harada, T. Tanada, and A. Yoshida (2011), Fluid-induced swarm earthquake sequence revealed by precisely determined hypocenters and focal mechanisms in the 2009 activity at Hakone volcano, Japan, *J. Geophys. Res.*, *116*, B04308, doi:10.1029/2010JB008036.

R. E. Abercrombie, Department of Earth Sciences, Boston University, Boston, MA 02478, USA.

X. Chen and P. M. Shearer, Scripps Institution of Oceanography, University of California, San Diego, La Jolla, CA 92093, USA. (xic002@ucsd.edu)